Transit Detection of Exoplanet WASP-33b

Umran Haji
*University of California, Berkeley, Department of Astronomy**

We observed a transit of the planet WASP-33b on the night of October 18-19, 2018 in the V-band using a 30-inch optical telescope at Leuschner Observatory. We successfully detected a transit and fit a simple model to the resulting lightcurve using a Markov chain Monte Carlo simulation to estimate the planet-star radius ratio. Using previous constraints on the radius of the host star and the mass of the planet, we estimate a planetary radius of $1.76^{+.053}_{-.055}\ R_J$ and a density of $0.385^{+.050}_{-.054}\ \rho_J$.

I. INTRODUCTION AND DATA ACQUISITION

We observed a transit of WASP-33b that occurred from approximately 11:00 PM to 1:30 AM PST (6:00 AM to 8:30 AM UTC) on the night of October 18-19, 2018. We obtained approximately 660 V-band images of WASP-33 and nearby reference stars using exposure times from one to four seconds. "Dark" exposures were taken immediately following the observation (20 images for each exposure time), and we used flat-field images taken in 2016 for calibration purposes (described in section II).

We experienced minor technical difficulties throughout the observation. The primary issue of note was that the observatory dome failed to automatically move with the telescope, leading to a blockage of the line of sight by the dome and thus several minutes without any data (visible as a gap in the middle of Figure 7). However, our ability to detect the transit was not hindered.

In this work, we discuss the analysis and results of our photometry data.

II. FLAT FIELD CALIBRATION

The first step in preparing to process our data is to correct for non-uniform responses across the telescope's CCD. Under ideal circumstances, in which the sensitivity of a pixel to photons is uniform across all pixels, our model for the response R_i (in arbitrary units) of a given pixel i is as follows:

$$R_i = GN_i + d_i + r$$

where N_i is a random variable representing the number of photo-electrons collected by pixel i, G is a constant gain factor with units such that when multiplied by N_i it yields a value with the units of R_i, d_i is a random variable representing the response in the pixel due to dark current, and r is a constant read bias.

However, not all pixels are equally sensitive to photons. We can model this by modifying the equation as follows:

$$R_i = G_iN_i + d_i + r \tag{1}$$

where G_i is a now an effective gain factor that varies from pixel to pixel but is assumed to be constant within each pixel through time.

In this section, we detail a process for correcting an image for the differing G_i values.

Taking expectation values of both sides of equation (1) yields:

$$\begin{aligned}\mathrm{E}(R_i) &= \mathrm{E}(G_iN_i + d_i + r)\\ &= G_i\mathrm{E}(N_i) + \mathrm{E}(d_i) + r\end{aligned} \tag{2}$$

Previous work has shown that the number of photons in a given wavelength range hitting a detector in some given time interval is well-modeled as a Poisson random variable. Thus, N_i is a Poisson random variable whose expectation is some constant μ_i. In the special case in which the telescope is pointing at a uniformly bright source, as in the case of a flat field image, each pixel is "seeing" the same apparent brightness, and thus this value is some constant independent of i, which we will call μ. Thus equation (2) yields:

$$\mathrm{E}(R_i) = G_i\mu + \mathrm{E}(d_i) + r \tag{3}$$

A "dark" exposure can be modeled as the sum of a dark current and read bias; i.e., if D_i is a random variable representing the response in pixel i during a dark exposure, then we can write:

$$D_i = d_i + r \tag{4}$$

and thus the expected value of pixel i's reponse during a dark exposure is:

$$\mathrm{E}(D_i) = \mathrm{E}(d_i) + r$$

Let $Q_i = R_i - D_i$ be the value of pixel i in a dark-subtracted image. Then the expected response in a dark-subtracted flat field is given by:

$$\begin{aligned}\mathrm{E}(Q_i) &= \mathrm{E}(R_i) - \mathrm{E}(D_i)\\ &= G_i\mu + \mathrm{E}(d_i) + r - \mathrm{E}(d_i) - r\\ &= G_i\mu\end{aligned} \tag{5}$$

Next, let

$$Q_{avg} \equiv \frac{1}{n_p}\sum_{i=1}^{n_p} Q_i$$

* uhaji@berkeley.edu

be the average dark-subtracted response across the entire image, where n_p is the number of pixels. The expected vale of Q_{avg} is

$$\mathrm{E}(Q_{avg}) = \frac{1}{n_p}\sum_{i=1}^{n_p}\mathrm{E}(Q_i) = \frac{\mu}{n_p}\sum_{i=1}^{n_p}G_i \tag{6}$$

Then, combining equations (5) and (6) yields:

$$\mathrm{E}(Q_i) = \frac{n_p G_i}{\sum_{i=1}^{n_p} G_i} E(Q_{avg}) \tag{7}$$

Equation (7) is the key to estimating the relative gain of each pixel; according to (7), on average, the value of a pixel in a dark-subtracted flat field should be linearly related to the average response across all the pixels in the *entire* dark-subtracted flat field. The slope, $n_p G_i / \sum_{i=1}^{n_p} G_i$, depends on how large pixel i's gain is relative to the average gain of all the pixels in the field; e.g., if G_i is less than the average gain, we will have $n_p G_i / \sum_{i=1}^{n_p} G_i < 1$, and if G_i is greater than the average gain, we will have $n_p G_i / \sum_{i=1}^{n_p} G_i > 1$.

As an example, Figure 1 shows 51 dark-subtracted values (we had 51 V-band flat-field images at our disposal) of one of the CCD's corner pixels plotted against the average value across the entire dark-subtracted image for each of those 51 images. The black line is a least-squares fit. For this particular pixel, we find a best-fit slope value of approximately 0.70, suggesting that the gain of this pixel is approximately 0.70 times the average gain.

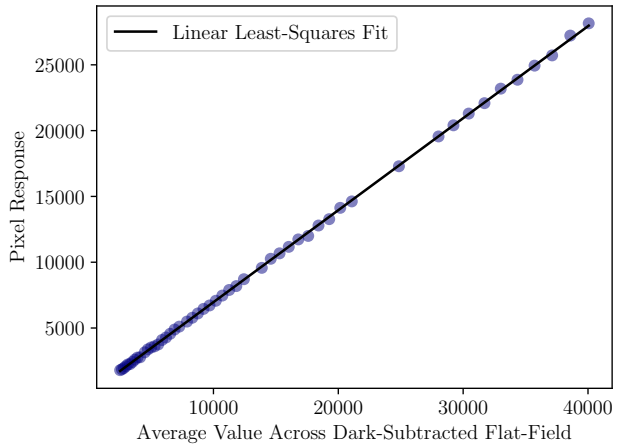

FIG. 1. The response of a particular corner pixel as a function of the average response of the entire CCD.

Repeating this process for each of the ∼2,600,000 pixels in the field yields a "map" of all the relative gains, shown in Figure 2, which is used to correct our images.

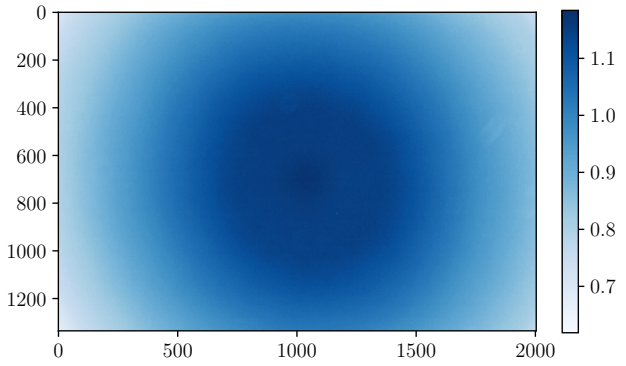

FIG. 2. The relative gains of the pixels in the CCD. A dark-subtracted image can be divided by this relative gain field to correct for differing responses across the CCD.

III. OBTAINING A LIGHT CURVE

The immediate next step before proceeding with any further analysis is to "correct" the images by subtracting from each frame the mean "dark" frame corresponding to its exposure length, and then dividing the result by the estimated relative gain values found in section II. After correcting all frames, we prepare a light curve via the steps detailed in this section.

A. Star Tracking

The stars in the field of view drift over time due to imperfect tracking by the telescope. Thus, the stars' positions need to be tracked so that their fluxes can be calculated.

Our target or "science" star is the brightest star in the image by far; thus, locating it is accomplished by simply locating the brightest pixel in each frame. To locate our chosen reference star, we take advantage of the fact that the stars' relative positions are fixed; Figure 3 shows one of our corrected frames, with the science star in the yellow box and our reference star in the blue box. The grey arrow represents the vector from the science star to the reference star. This vector should remain constant through time, aside from small fluctuations on the scale of a few pixels caused by noise. Hence, once the science star is identified in a frame, the reference star is found by drawing this vector from the science star, extracting a small region centered at the head of the vector, and calculating the centroid of that region.

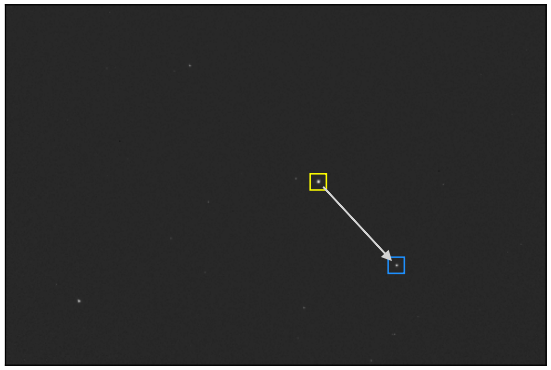

FIG. 3. This image is one of our "corrected" (i.e. dark-subtracted and gain-divided) frames. The yellow box indicates the science star, while the blue box indicates the reference star. The grey arrow represents the vector connecting the two, which is used to locate the reference star in each image.

Once each star is located in a given image, a 60-by-60 pixel square cutout centered on the star's centroid is extracted from the image and saved for later analysis.

B. Aperture Optimization and SNR Calculation

After extracting cutouts of each star from each of our ∼660 frames, stellar fluxes must be calculated in order to conduct relative aperture photometry. Doing so requires choosing an appropriate aperture within which to sum pixel flux values. Within each frame, we calculate stellar fluxes using circular apertures centered on the centroids of the science star and reference star, respectively. The radius of the aperture is chosen so as to optimize the signal-to-noise ratio (SNR) of the reference star, by a process that we describe below.

In a corrected image, the flux F_i in a pixel i can be modeled as the sum of a Poisson term caused by photons from the star and a "background" term that encapsulates contributions from a multitude of other sources, including background light on the sky, fluctuations in the dark current, and so on. We denote this background term as B_i. Given an aperture that includes n pixels, the signal S that is due to the starlight within that aperture is estimated by subtracting from each F_i the expected value of the background flux, $\mathrm{E}(B_i)$ and summing the result:

$$S = \sum_{i=1}^{n} F_i - \mathrm{E}(B_i) \tag{8}$$

For a small neighborhood around a given star in a given frame, we expect that $\mathrm{E}(B_i)$ is a constant independent of i, and therefore we can estimate $\mathrm{E}(B_i)$ for the pixels within the aperture using pixels outside the aperture that have negligible stellar flux and are dominated by the background flux. Our choice of cutout size was informed by this; Figure 4 shows the flux values for the science star in one of our 60-by-60 cutouts, summed along one of the axes. The flux falls off dramatically after a few pixels, leaving the edges of the cutout comfortably separated from the star. As a result, the edge pixels are sufficiently far away as to be dominated by background flux.

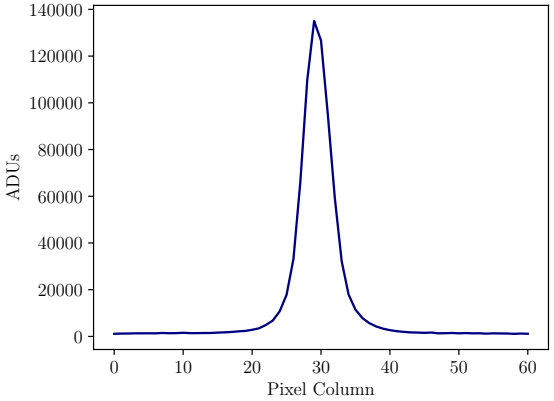

FIG. 4. The flux of the science star in one cutout, in analog-to-digital units, summed along one axis. The flux falls off dramatically after just a few pixels, allowing the edges of the cutout to be used for background estimation.

To estimate $\mathrm{E}(B_i)$ for each cutout, we use the median of the flux values along the cutout's edges. We use the median as an estimator of $\mathrm{E}(B_i)$ in order to guard against outliers caused by "hot" pixels, "dead" pixels, cosmic rays, and other exceptional phenomena. The distribution of the background flux is approximately symmetric aside from occasional outliers. This fact is exemplified in Figure 5, which shows the background flux distribution for a typical cutout. This fact implies that the sample median is a reasonable stand-in for the sample mean.

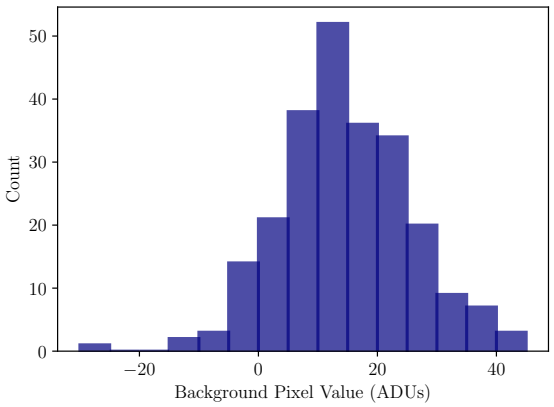

FIG. 5. The distribution of background fluxes calculated from the edge pixels in one 60-by-60 cutout around the reference star. The background flux is approximately symmetrically distributed except for an occasional outlier.

Having calculated S, the next step is to calculate the variance on S, i.e. σ_S^2, the square root of which is the "noise" in the SNR calculation. Since S is the sum of two terms that are uncorrelated (since the intrinsic stellar flux has nothing to do with the background flux), σ_S^2 is likewise the sum of a Poisson term and a term from the background noise. The Poisson variance is equal to the expectation value and can hence be estimated by the value of S itself. Meanwhile, the background flux B_i in each pixel is assumed to be independent of the background flux in every other pixel, and hence the background variance term is the number of pixels times the background variance:

$$\sigma_S^2 = \frac{S}{G} + n\sigma_B^2 \tag{9}$$

where G is the overall gain factor of 1.6 electrons per ADU, and σ_B^2 is estimated by the sample variance of the flux values along the edges of the cutout.

Thus, for any aperture containing n pixels, the SNR is readily calculated via equations (8) and (9).

In general, starting with a small aperture and increasing the radius causes the SNR to increase due to the greater amount of stellar flux captured within the aperture, until such a point where increasing the radius merely captures pixels far away from the star whose negligible stellar flux contribution is outweighed by their contribution to the background variance. Hence, there exists an optimal aperture size that maximizes SNR. Figure 6 shows the relationship between aperture radius and SNR for one of our reference star cutouts.

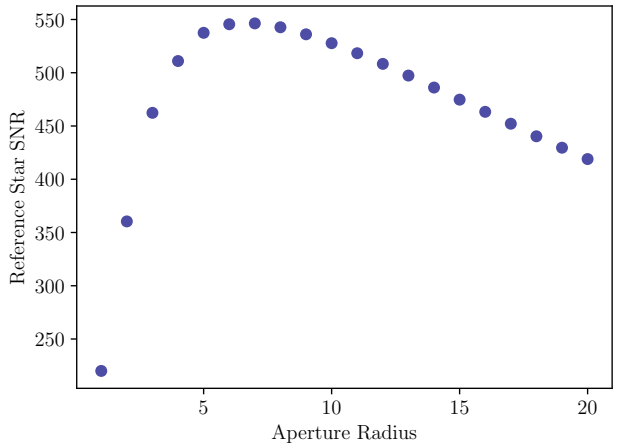

FIG. 6. The SNR for the reference star in one image as a function of the radius of the aperture within which the flux is summed. The radius that maximizes SNR is chosen as the aperture radius for both stars in the image.

In general, the optimal aperture size changes from frame to frame. Thus, within in each frame, a frame-specific optimal radius is calculated based on the reference star, and values of S and σ_B are calculated and saved for each star using an aperture of that size.

C. Flux Ratio and Uncertainty Calculation

After obtaining signal and noise values for each star in each of the ∼660 frames, science star signal values are divided by the corresponding reference star signal values to find the ratio $R = S_{sci}/S_{ref}$. Then, we make the assumption that the noise of the science star signal, $\sigma^2_{S_{sci}}$, is independent of the noise of the reference star signal, $\sigma^2_{S_{ref}}$. This is a reasonable assumption since the Poisson contributions to each one clearly come from independent Poisson distributions (they are different stars), and the background noise is independent among different regions of the image. Under this assumption, the relative errors add in quadrature to produce the relative error on R:

$$\left(\frac{\sigma_R}{R}\right)^2 = \left(\frac{\sigma_{S_{sci}}}{S_{sci}}\right)^2 + \left(\frac{\sigma_{S_{ref}}}{S_{ref}}\right)^2$$

We thereby solve for the values of σ_R for each frame, which form the error bars for our final lightcurve. This lightcurve is shown in Figure 7, where the horizontal axis is the number of seconds since the start of the day in UTC and the vertical axis is the flux ratio R.

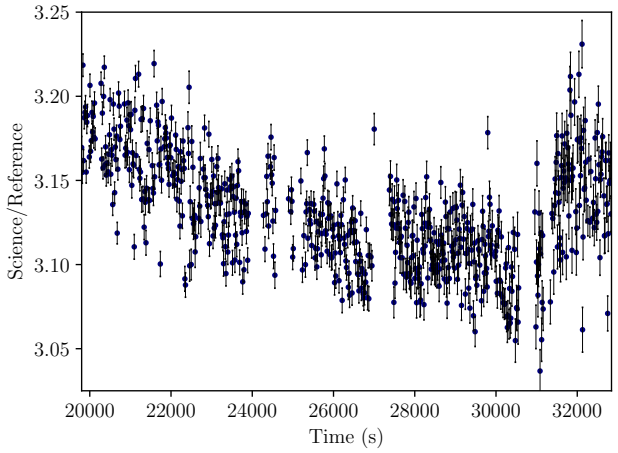

FIG. 7. Light curve showing the ratio of the background-subtracted flux of the science star to that of the reference star. The horizontal axis is the number of seconds since midnight in UTC.

IV. MODEL-FITTING AND PARAMETER ESTIMATION

In Appendix A, we derive a simple model for the shape of the lightcurve under several assumptions about the nature of the transit. The model is parameterized in terms of t_0, the start time of ingress, T, the time between the end of ingress and the start of egress, and r/R, the ratio of the planet radius r to the star radius R (not to be confused with the flux ratio R in section III C).

A Markov chain Monte Carlo procedure is employed to fit the model. We assume that each data point is drawn from a normal distribution with mean equal to the deterministic model value and standard deviation equal to the error bar on the data point. We use uninformative prior distributions that are readily estimated from inspection of the lightcurve data, a virtue of our parameterization; t_0 is taken to be uniform on $[21000, 23000]$, T is uniform on $[7000, 11000]$, and r/R is uniform on $[.01, .2]$.

We generate 100,000 model curves and plot a random sample of 500 of these in Figure 8.

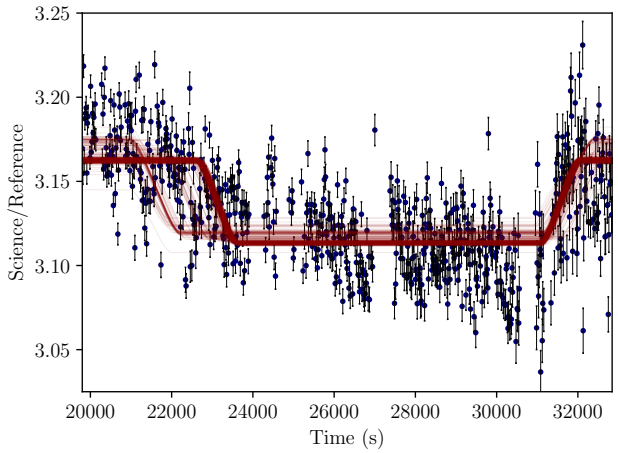

FIG. 8. Our light curve overlain with a random sample of 500 model curves, in red, from the MCMC.

The radius ratio is readily estimated from the generated models. Figure 9 shows the distribution of r/R as well as an approximate 1σ region; from this, we estimate a radius ratio of $0.125^{+.0018}_{-.0015}$.

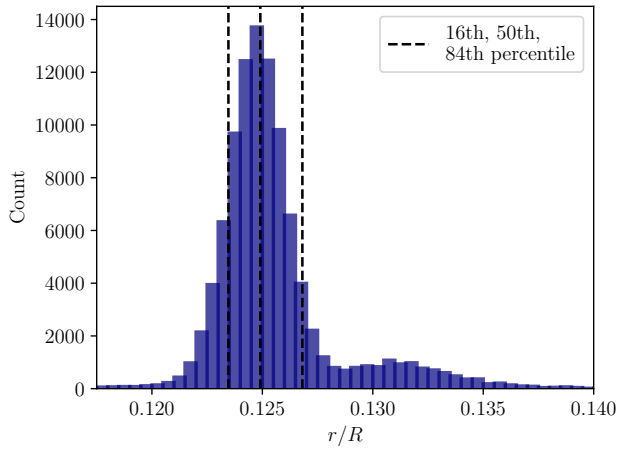

FIG. 9. Approximate posterior distribution of the planet-to-star radius ratio from the MCMC. The dashed lines show the median and approximate 1σ region.

Cameron et al. [1] found a radius of 1.444 ± 0.034 $R_\odot$ for the host star. To estimate the absolute radius of the planet, we multiply each of our 100,000 values for r/R by a random value drawn a normal distribution with $\mu = 1.444$ and $\sigma = 0.034$ $R_\odot$. Figure 10 shows the resultant distribution for r in solar radii. From this distribution, we estimate a 1σ region of $0.181^{+.0054}_{-.0056}$ $R_\odot$, or, in Jupiter radii, $1.76^{+.053}_{-.055}$ R_J.

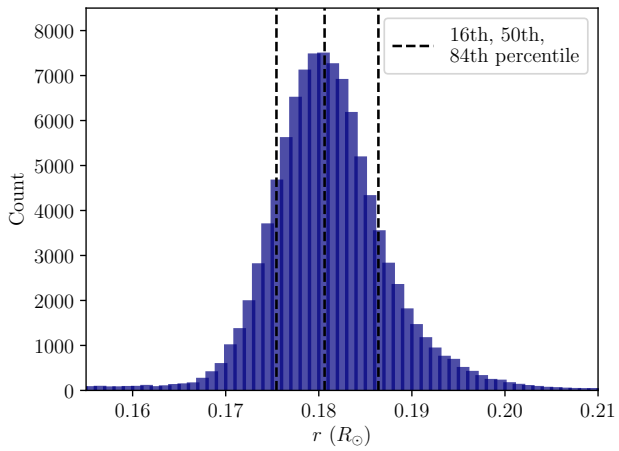

FIG. 10. Distribution of the planet radius in solar radii, obtained by multiplying each value from our r/R distribution by a value drawn from a normal distribution representing the star's radius using results from [1]. The dashed lines show the median and approximate 1σ region.

Lehmann et al. [2] used radial velocity measurements to find a planetary mass of 2.1 ± 0.2 Jupiter masses. We use this and our radius distribution to estimate the planet density; we draw 100,000 values from a normal distribution with $\mu = 2.1$ and $\sigma = 0.2$ R_J, pairing each one with a radius value and finding the density in units of Jupiter densities by

$$\frac{\rho}{\rho_J} = \frac{M}{M_J}\left(\frac{R_J}{R}\right)^3$$

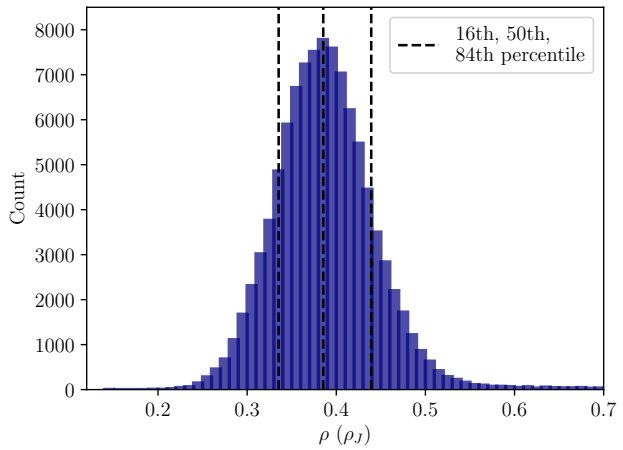

FIG. 11. Distribution of the planet density in Jupiter densities, obtained by multiplying each value from our radius distribution by a value drawn from a normal distribution representing the planet's mass, using results from [2]. The dashed lines show the median and approximate 1σ region.

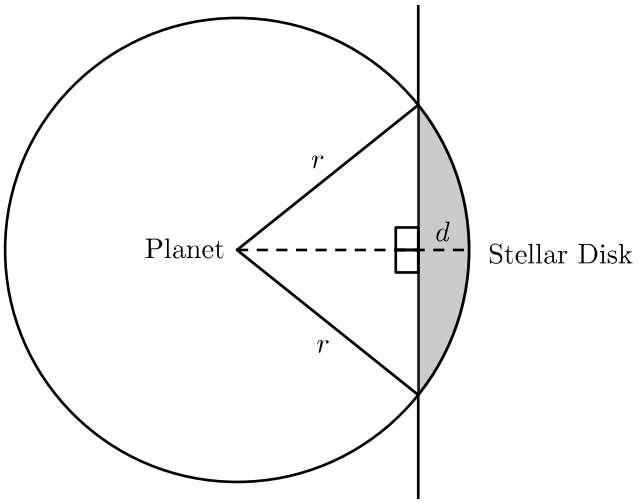

FIG. 12. Our model for the amount of light blocked by the planet given the projected distance d of its leading edge from the edge of the stellar disk.

Figure 11 shows the resulting density distribution. We find an approximate 1σ region of $0.385^{+.050}_{-.054}$ ρ_J. The planet is significantly less dense than Jupiter, implying that it is likely a gaseous planet.

V. CONCLUSION

We were able to definitively detect WASP-33b and estimate some of its general properties. However, our work is limited by several issues, foremost among them being the imprecision of our instrument. A secondary issue is the fact that WASP-33 is known to be a variable star with periodicities on the order of one hour and amplitudes on the order of 1 mmag [3], which may have contributed to the obscuring of the transit, whose amplitude is ∼10 mmag.

Appendix A: A Simple Light Curve Model

In this section, we develop a simple analytical model for the relative brightness of a star during a transit, to be fit to our data using a Markov chain Monte Carlo (MCMC) procedure.

We approximate the interface between the projected disks of the star and planet as a straight line, a valid assumption if the radius of the star is much greater than the radius of the planet and the planet's orbital inclination is nearly 90 degrees. We ignore possible inaccuracies caused by non-90 degree inclination and the straight line assumption because we expect our instrumentation to be too imprecise to capture these effects.

During ingress, the area of the stellar disk that is blocked by the planet is the area of the shaded circular segment in Figure 12. In general, the area of such a segment can be expressed in terms of its width d as

$$A = r^2 \arccos\left(1 - \frac{d}{r}\right) - (r-d)\sqrt{2rd - d^2}$$

for $d \in [0, 2r]$ (as we will see, it is more convenient to use the fractional area $a = A/\pi r^2$).

The width d depends on the tangential velocity of the planet on the sky and the time elapsed since the start of ingress. Under the assumption that the planet's orbit is nearly circular and its semi-major axis is reasonably large compared to the radius of the star, the tangential velocity can be approximated as a constant v, and thus $d \approx vt$, where $t = 0$ is the time when the right edge of the planetary disk crosses the vertical line. Hence, we have

$$a(t) = \frac{1}{\pi}\left[\arccos\left(1 - \frac{vt}{r}\right) - \left(1 - \frac{vt}{r}\right)\sqrt{2\frac{vt}{r} - \left(\frac{vt}{r}\right)^2}\right] \tag{A1}$$

for $t \in [0, \Delta t]$ where Δt is the duration of ingress, i.e. the time it takes for the left edge of the planetary disk to cross the vertical line.

Evidently, (A1) can be written in terms of the dimensionless quantity $x = vt/r$, which, by inspection of the inverse cosine term, is allowed to range from 0 to 2:

$$a(x) = \frac{1}{\pi}\left[\arccos(1-x) - (1-x)\sqrt{2x - x^2}\right] \tag{A2}$$

for $x \in [0, 2]$ where $x = 2$ corresponds to $t = \Delta t$.

We make this equation more general by letting ingress start at some dimensionless "time" $x = x_0$. Then,

$$a_{\text{in}}(x) = a(x - x_0) \tag{A3}$$

for $x \in [x_0, x_0 + 2]$.

Now, let $l = x_2 - (x_0 + 2)$ be the dimensionless time between the end of ingress and the start of egress (which is at some x_2). Then we have $a(x) = 1$ for $x \in (x_0 + 2, x_0 + 2 + l)$.

Finally, the fraction of the planet's area that is blocking the star as a function of x during egress is the same as during ingress, but in reverse. So, we obtain $a(x)$ for egress by "flipping" and phase-shifting (A2) to obtain:

$$\begin{aligned} a_{\text{out}}(x) &= a(-(x - x_2) + 2) \\ &= a(-(x - (x_0 + 2 + l)) + 2) \end{aligned} \tag{A4}$$

for $x \in [x_0 + 2 + l, x_0 + 4 + l]$. The extra $+2$ added at the end arises because after flipping $a(x)$ over the ordinate axis, its domain is now $[-2, 0]$ rather than $[0, 2]$ and it must be shifted to the right by 2.

Finally, we can write a piecewise function for the apparent brightness B of the star over time. Our instrumentation being far too imprecise to detect variations due to limb darkening, we assume the apparent brightness is solely determined by the blocking area. Hence,

$$B = B_0 \left(1 - \left(\frac{r}{R}\right)^2 a\right) \tag{A5}$$

where

$$a = \begin{cases} 0 & x < x_0 \\ a_{\text{in}}(x) & x \in [x_0, x_0 + 2] \\ 1 & x \in (x_0 + 2, x_0 + 2 + l) \\ a_{\text{out}}(x) & x \in [x_0 + 2 + l, x_0 + 4 + l] \\ 0 & x > x_0 + 4 + l \end{cases} \tag{A6}$$

for some constant intrinsic brightness B_0 and stellar radius R.

Figure 13 shows the functional form of our light curve model given by (A5) and (A6), with arbitrary scales on the axes.

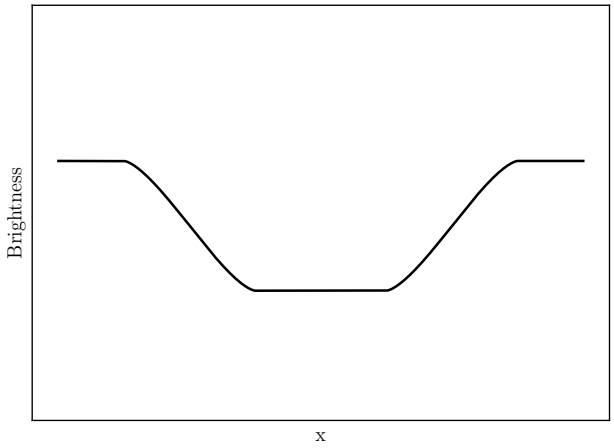

FIG. 13. The functional form of our model for the brightness of a star during a transit.

The dimensionless equation is useful, as it can be manipulated in various ways to re-parameterize the problem depending on the parameters one wishes to determine via a model-fitting procedure. In our case, we primarily seek to estimate the ratio r/R without having any information about the parameter v. It turns out that the model can be completely parameterized in terms of the start time of ingress t_0, the time T between the end of ingress and start of egress, the ratio r/R, and the pre- and post-transit brightness B_0, as we now demonstrate.

Observe that the time interval T is the time it takes the right edge of the planet to cross from the left edge of the stellar disk to the right edge, and thus $T = 2R/v$, again relying on our assumption of constant tangential velocity. Now, if the model is written in a form that takes values of t as arguments rather than values of x, we obtain the dimensionless value $x(t)$ by multiplying t by v/r. This fraction can be written in terms of our chosen input parameters, as follows:

$$\begin{aligned} T = \frac{2R}{v} \rightarrow v = \frac{2R}{T} \rightarrow \frac{v}{r} &= \frac{2}{T}\frac{R}{r} \\ \rightarrow \frac{v}{r} &= \frac{2}{T(r/R)} \end{aligned}$$

and thus we have:

$$x(t \mid T, r/R) = \frac{2}{T(r/R)}\, t \tag{A7}$$

So, given values for the parameters T and r/R, obtaining a model prediction for time t amounts to passing t into equation (A7) and then passing the resultant x to (A5) and (A6), with bounds determined by:

$$\begin{aligned} x_0 &= x(t_0 \mid T, r/R) \\ l &= x(T \mid T, r/R) = \frac{2R}{r} \end{aligned}$$

Thus, the model

$$\begin{aligned} B(t) &= B(t \mid t_0, T, r/R, B_0) \\ &= B_0 \left(1 - \left(\frac{r}{R}\right)^2 a\right) \\ &= B_0 \left(1 - \left(\frac{r}{R}\right)^2 a\left(x(t \mid T, r/R) \mid x(t_0), x(T)\right)\right) \end{aligned}$$

can be readily used as the basis for an MCMC procedure.

[1] A. Collier Cameron, E. Guenther, B. Smalley, I. McDonald, L. Hebb, J. Andersen, Th. Augusteijn, S. C. C. Barros, D. J. A. Brown, W. D. Cochran, M. Endl, S. J. Fossey, M. Hartmann, P. F. L. Maxted, D. Pollacco, I. Skillen, J. Telting, I. P. Waldmann, R. G. West; Line-profile tomography of exoplanet transits II. A gas-giant planet transiting a rapidly rotating A5 star, Monthly Notices of the Royal Astronomical Society, Volume 407, Issue 1, 1 September 2010, Pages 507-514, https://doi.org/10.1111/j.1365-2966.2010.16922.x

[2] H. Lehmann, E. Guenther, D. Sebastian, M. Döllinger, M. Hartmann, D.E. Mkrtichian; Mass of WASP-33b, Astronomy and Astrophysics, Volume 578, :L4, 4 June 2015, https://doi.org/10.1051/0004-6361/201526176

[3] A. M. S. Smith, D. R. Anderson, I. Skillen, A. Collier Cameron, B. Smalley; Thermal emission from WASP-33b, the hottest known planet, Monthly Notices of the Royal Astronomical Society, Volume 416, Issue 3, 21 September 2011, Pages 20962101, https://doi.org/10.1111/j.1365-2966.2011.19187.x